https://doi.org/10.5194/bg-2021-152
Preprint. Discussion started: 17 June 2021

Biogeosciences Discussions

Resolving temperature limitation on spring productivity in an evergreen conifer forest using a model-data fusion framework

Stephanie G. Stettz[1], Nicholas C. Parazoo[2], A. Anthony Bloom[2], Peter D. Blanken[3], David R. Bowling[4], Sean P. Burns[3,5], Cédric Bacour[6], Fabienne Maignan[7], Brett Raczka[5] , Alexander J. Norton[2], Ian Baker[8], Mathew Williams[9,10], Mingjie Shi[11], Yongguang Zhang[12], Bo Qiu[12]

[1] Department of Earth System Science, University of California Irvine, Irvine, California, USA
[2] Jet Propulsion Laboratory, California Institute of Technology, Pasadena, California, USA
[3] Department of Geography, University of Colorado Boulder, Boulder, Colorado, USA
[4] School of Biological Sciences, University of Utah, Salt Lake City, Utah, USA
[5] National Center for Atmospheric Research, Boulder, Colorado, USA
[6] NOVELTIS, 153 rue du Lac, 31670 Labège, France
[7] Laboratoire des Sciences du Climat et de l'Environnement, LSCE/IPSL, CEA-CNRS-UVSQ, Université Paris-Saclay, Gif-sur-Yvette, France
[8] Cooperative Institute for Research in the Atmosphere, Colorado State University, Fort Collins, Colorado, USA
[9] School of GeoSciences and National Centre for Earth Observation, University of Edinburgh, Edinburgh, UK
[10] National Centre for Earth Observation, Edinburgh EH9 3FF, Edinburgh, UK
[11] Pacific Northwest National Laboratory, 902 Battelle Blvd, Richland, WA 99354
[12] International Institute for Earth System Sciences, Nanjing University, Nanjing, Jiangsu Province, China

Correspondence to: Stephanie Stettz (sstettz@uci.edu)

Abstract

The flow of carbon through terrestrial ecosystems and the response to climate is a critical but highly uncertain process in the global carbon cycle. However, with a rapidly expanding array of in situ and satellite data, there is an opportunity to improve our mechanistic understanding of the carbon (C) cycle's response to land use and climate change. Uncertainty in temperature limitation on productivity pose a significant challenge to predicting the response of ecosystem carbon fluxes to a changing climate. Here we diagnose and quantitatively resolve environmental limitations on growing season onset of gross primary production (GPP) using nearly two decades of meteorological and C flux data (2000-2018) at a subalpine evergreen forest in Colorado USA. We implement the CARDAMOM model-data fusion network to resolve the temperature sensitivity of spring GPP. To capture a GPP temperature limitation—a critical component of integrated sensitivity of GPP to temperature—we introduced a cold temperature scaling function in CARDAMOM to regulate photosynthetic productivity. We found that GPP was gradually inhibited at temperature below 6.0 °C (± 2.6 °C) and completely inhibited below -7.1 °C (± 1.1 °C). The addition of this scaling factor improved the model's ability to replicate spring GPP at interannual and decadal time scales (r = 0.88), relative to the nominal CARDAMOM configuration (r = 0.47), and improved spring GPP model predictability outside of the data assimilation training period (r = 0.88) . While cold temperature limitation has an important influence on spring GPP, it does not have a significant impact on integrated growing season GPP, revealing that other environmental controls, such as precipitation, play a more important role in annual productivity. This study

https://doi.org/10.5194/bg-2021-152
Preprint. Discussion started: 17 June 2021

highlights growing season onset temperature as a key limiting factor for spring growth in winter-dormant evergreen forests, which is critical in understanding future responses to climate change.

1. Introduction

Northern hemisphere evergreen forests contribute significantly to terrestrial carbon (C) storage and exchange (Beer et al., 2010; Thurner et al., 2014). High-elevation evergreen forests show increasing gross primary productivity (GPP) with increasing temperature driven in large part by earlier growing seasons (Myneni et al., 1997; Randerson et al., 1999; Forkel et al., 2016; Winchell et al., 2016, Lin et al., 2017). However, the response of gross and net C fluxes to warming remains uncertain, especially in subalpine temperate forests, which can experience freezing temperature while still absorbing large amounts of sunlight; both these factors ultimately influence the timing and magnitude of GPP (Bowling et al. 2018). In particular, warmer springs can also lead to earlier snowmelt, which can reduce spring C uptake through increased surface exposure to colder ablation-period air temperatures (Winchell et al., 2016), and can reduce summer C uptake via drought (Hu et al., 2010). Many subalpine forests in western North America are also highly water limited, with warming and earlier snow melt creating accumulated water deficits, increased drought stress, and growing season C uptake losses (Wolf et al., 2016; Sippel et al., 2017; Buermann et al., 2018, Goulden and Bales, 2019); these factors ultimately make subalpine forest ecosystems sensitive to the direct and indirect effects of climate change and other disturbances, including the effects of droughts, fires and insect infestations (Frank et al., 2014; Knowles et al., 2015). The uncertainty in the temperature sensitivity of springtime GPP, increasing vulnerability to disturbance, and GPP modeling challenges (Anav et al., 2015) create urgency to improve our ability to observe and model these ecosystems to understand how C exchange will be altered in a warming climate.

Fortunately, availability of long term ecosystem observations is improving. The expansion of international flux tower networks over the last three decades (e.g. AmeriFlux, FLUXNET, ChinaFLUX, ICOS) has greatly improved C flux sampling across global ecosystems at 1 km scale (Baldocchi 2008; Baldocchi et al., 2018), and the number of spaceborne sensors continues to grow, allowing global estimation of gross primary production (GPP) and net ecosystem C exchange (NEE) over the last decade (e.g. Stavros et al., 2017; Sun et al., 2017; Schimel et al., 2019). While uncertainties in estimating C fluxes from in situ and satellite data remain a challenge, the expanding observational record offers a great opportunity to study the temperature sensitivity of subalpine forests at multiple temporal scales.

The range of modeling tools available to quantify and study major C pools under ever growing observational constraints is also increasing. Process-based models, in general terms, use explicit mathematical relationships to mechanistically describe bio-physical processes (Korzukhin et al., 1996; Huxman et al., 2003; Keenan et al., 2012). In contrast, model-data fusion (MDF) is a relatively new tool that alters model parameters to statistically reduce mismatches between observations and model predictions (Raupach et al., 2005; Wang et al., 2009; Keenan et al., 2012). MDF methods can be used to statistically represent the terrestrial C balance by generating optimized state and process variable parameterizations, with uncertainties, which best match the signal and noise in observations (Bloom et al., 2020).

https://doi.org/10.5194/bg-2021-152
Preprint. Discussion started: 17 June 2021

Models of varying complexity and assimilation capabilities have been used to study how C exchange varies with temperature in subalpine evergreen ecosystems (e.g., Moore et al., 2008; Scott-Denton et al., 2013; Knowles et al., 2018). Moore et al. (2008) used a simplified ecosystem function model and assimilated C flux data from the Niwot Ridge (US-NR1) subalpine evergreen forest AmeriFlux tower in Colorado to show the importance of accurate meteorological forcing for parameter optimization and the usefulness of assimilating C flux data for determining connections between the C and water cycles. Scott-Denton et al. (2013) integrated meteorological and flux data from 1999-2008 from the same site with an ensemble of more sophisticated Earth System Models (ESM) and showed higher rates of C uptake by the end of the 21st century associated with warming and lengthening growing seasons, and driven by greater increases of spring GPP relative to late season respiration.

Interestingly, model and empirical studies of the C flux response to climate at US-NR1 focus on the 2000-2011 period, which saw increasing summer drought coupled with sustained declines in spring temperature and GPP. US-NR1 has since experienced a gradual recovery of spring GPP with increased spring warming throughout 2011-2018 (Figure 1), which begs the question: what is the temperature sensitivity of spring GPP over multiple decades of spring cooling and warming at US-NR1, and how well can data-constrained models reproduce long term variability? To answer this question, we combine a mechanistic ecosystem C model (Data Assimilation Linked Ecosystem Carbon, DALEC2; Williams et al., 2005; Bloom et al., 2016) with the CARbon DAta-MOdel fraMework (CARDAMOM; Bloom and Williams, 2015; Bloom et al., 2020) driven by observed meteorological forcing and constrained against eddy covariance fluxes at US-NR1, to investigate the temperature sensitivity of this subalpine evergreen forest at seasonal and interannual timescales. We introduce a new cold temperature limitation function, trained on observed temperature, for more realistic simulation of spring GPP onset. The use of high quality and long term (2000-2018) meteorology and partitioned GPP data at US-NR1 to drive and constrain the model enables robust statistical analysis of interannual variability (IAV), and assessment of "model predictability" through training and validation against subsets of data. We also leverage a recent model intercomparison study (Parazoo et al., 2020), driven by site level meteorological data at US-NR1, to provide a model benchmark assessment, and extract any common environmental controls on modeled GPP. Finally, we examine whether decadal flux tower-derived GPP observations are sufficiently robust to match and predict seasonal to annual GPP. Given the complexity of carbon-water cycle interactions during the growing (summer) season in this highly water limited ecosystem, and the relatively weak correlation between tower-derived spring and summer GPP ($r = -0.31$, $p = 0.20$), we focus on spring GPP-temperature interactions, with the aim to resolve just one piece of the larger, complex problem of understanding changes in C uptake in a subalpine evergreen ecosystem.

2. Materials & Methods

2.1. Study Site: Niwot Ridge, CO., USA

Our study focuses on an AmeriFlux (https://ameriflux.lbl.gov/) core site in Niwot Ridge, Colorado, USA (US-NR1, 40°1'58''N; 105°32'47'' W), where a tower-based eddy covariance system has been continuously measuring the net ecosystem exchange (NEE) of carbon dioxide over a subalpine forest since November 1998. The

https://doi.org/10.5194/bg-2021-152
Preprint. Discussion started: 17 June 2021

112 26 m tall tower is located in a high elevation (3050 m) subalpine site in the Rocky Mountains of Colorado (Monson
113 et al., 2002). Located in an evergreen needleleaf (ENF) ecosystem, the dominant tree species include lodgepole pine
114 (*Pinus contorta*), subalpine fir (*Abies lasiocarpa*), and Engelmann spruce (*Picea engelmannii*) (Turnipseed et al.,
115 2002; Turnipseed et al., 2004). Average annual precipitation is 800 mm, with a majority of precipitation falling in
116 the winter as snow (Greenland, 1989; Knowles et al., 2015), which creates a persistent winter snowpack from
117 November through early June (Bowling et al., 2018).

118 **2.2. Observations**

119 NEE measurements are screened for calm conditions using the standard u_{star} filtering, gap-filled, and
120 partitioned into GPP and ecosystem respiration based on the relationship between nighttime NEE
121 (photosynthetically active radiation, PAR < 50 μmol m^{-2} s^{-1}) and air temperature (Reichstein et al., 2005; Wulzler et
122 al., 2018). Monthly averages of GPP based on nighttime partitioning show similar seasonal structure to results found
123 using an alternative daytime partitioning algorithm (Lasslop et al., 2010), so only nighttime partitioned GPP data are
124 reported here. All GPP estimates are processed as half hourly means, then averaged monthly. Details on the flux
125 measurements, data processing and quality control are provided in Burns et al. (2015).

126 **2.3. The CARDAMOM Model-Data Fusion System**

127 The CARbon DAta-MOdel FraMework (CARDAMOM; Bloom et al., 2016; Yin et al., 2020; Exbrayat et
128 al., 2018; Smallman et al., 2017; Quetin et al., 2020; Lopez-Blanco et al., 2017; Famiglietti et al., 2020; Bloom et
129 al., 2020; amongst others) uses carbon cycle and meteorological observations to constrain carbon fluxes, states and
130 process controls represented in the DALEC2 model of terrestrial C cycling (Williams et al., 2005; Bloom and
131 Williams, 2015). Specifically, CARDAMOM uses a Bayesian model-data fusion approach to optimize DALEC2
132 time-invariant parameters (such as leaf traits, allocation and turnover times) and the "initial" C and H_2O conditions
133 (namely biomass, soil and water states at the start of the model simulation period).
134 The DALEC model (Williams et al., 2005; Rowland et al. 2014; Fox et al., 2009; Richardson et al., 2010;
135 Famiglietti et al., 2020; Bloom & Williams, 2015; amongst others) is a box model of C pools connected via fluxes
136 that has been used to evaluate terrestrial carbon cycle dynamics across a range of ecosystems and spatial scales. In
137 all site, regional, and global applications, DALEC parameters are subject to very broad, but physically realistic, prior
138 distributions, and independently estimated and constrained by available observations at each grid point. Here we use
139 DALEC version 2 (DALEC2; Yin et al., 2020; Quetin et al., 2020; Bloom et al., 2020); gross and net carbon fluxes
140 are determined as a function of 33 parameters, which comprise of 26 time-invariant parameters relating to
141 allocation, turnover times, plant traits, respiration climate sensitivities, water-use efficiency and GPP sensitivity to
142 soil moisture, and 7 parameters describe the initial conditions of live biomass pools (live biomass C, dead organic C
143 and plant-available H_2O). Within DALEC2, GPP estimates are generated in the aggregated canopy model (ACM,
144 Williams et al., 1997); the ACM is derived from simple functional relationships with environmental and plant
145 structural and biochemical information (Williams et al., 1997), that are produced from a sensitivity analysis of GPP
146 estimates from the more comprehensive SPA land surface model scheme (Williams et al., 1996, Williams et al.,

https://doi.org/10.5194/bg-2021-152
Preprint. Discussion started: 17 June 2021

2001). ACM GPP estimates are contingent on plant structural and biochemical variables (including LAI, foliar nitrogen and nitrogen-use efficiency) and meteorological forcings (total daily irradiance, maximum and minimum daily temperature, day length, atmospheric CO_2 concentration). In DALEC2, water limitation on ACM is prescribed as a linear response to soil water deficit (Bloom et al., 2020). For more details on the model-data fusion methodology and CARD ensembles, we refer the reader to Appendix A. For a comprehensive overview of DALEC2 model, we refer the reader to Bloom et al., (2020) and references therein.

2.4. Experiment Design

In order to develop model experiments that could reliably evaluate temperature-GPP interactions, we first examine the observed environmental controls on tower-derived GPP. We focus on GPP during spring, defined here in the traditional sense as the period from March-May, which encompasses the climatological onset of GPP and transition from dormant winter conditions to peak summer conditions (Fig 1A). Mean spring GPP exhibits large interannual variability (IAV) with both a small decreasing trend from 2000-2010 (-0.02 g C m^{-2} day^{-1} per year) and increasing trend from 2010-2018 (0.04 g C m^{-2} day^{-1} per year) (Fig. 1B). Comparison to tower observed temperature data (Fig. 1A and Fig. 2) shows that spring GPP is positively correlated to mean spring temperature (Pearson's linear r = 0.88) and summer (June-September) temperature (r = 0.08). Mean winter (December-February) precipitation also has a positive correlation with spring GPP, (r = 0.07, p = 0.77), but it is much smaller than spring temperature. At interannual timescales, mean annual GPP shows a small increasing trend (0.0072 g C m^{-2} day^{-1} per year) over the time period (Fig. S1), and largest correlation with winter (December – February) precipitation (Pearson's linear r = 0.63, Fig. S2) and shortwave irradiance (r = -0.30). In contrast, spring temperature shows little correlation with mean annual GPP (r = -0.03, p = 0.91). It appears that winter precipitation and total irradiance are the dominant drivers in annual productivity, both of which are correlated, while spring temperatures show a first order effect in driving spring GPP.

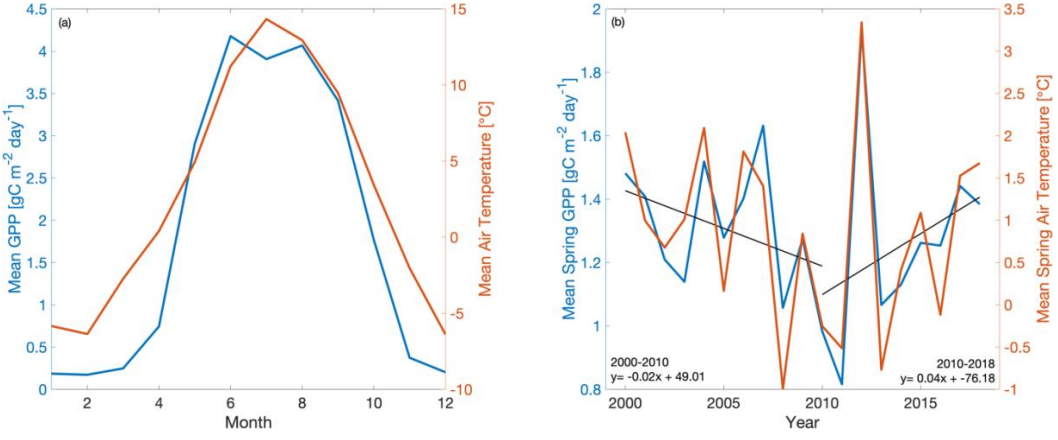

Figure 1. Time series of (a) mean monthly GPP (blue) and air temperature (orange) and (b) mean spring (March-May) GPP and air temperature at Niwot Ridge (US-NR1) from 2000-2018. GPP data are derived using a nighttime partitioning technique based on tower observations of NEE and air temperature.

https://doi.org/10.5194/bg-2021-152
Preprint. Discussion started: 17 June 2021

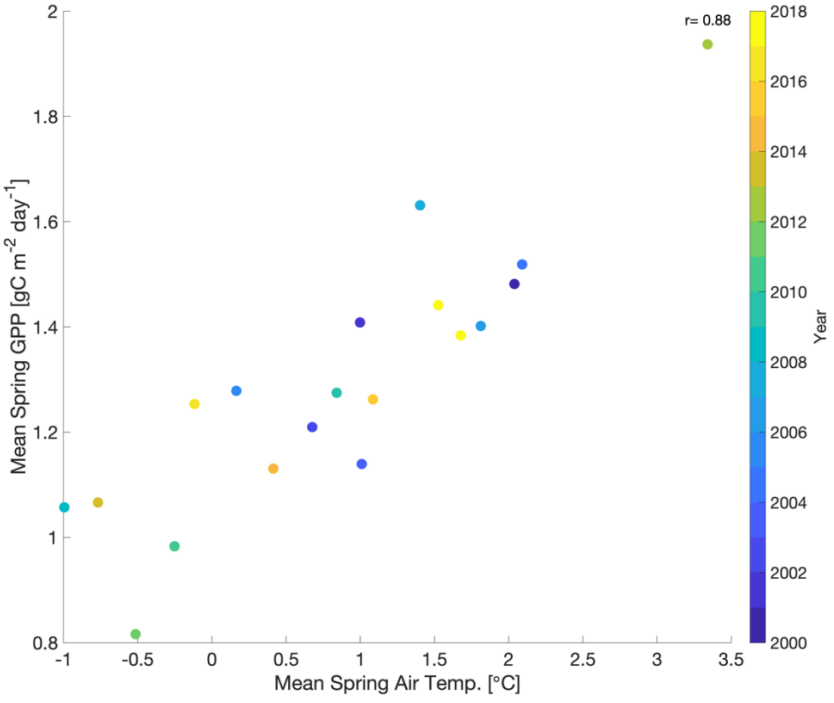

Figure 2. Scatterplot of mean spring (March-May) GPP with mean spring air temperature with the color bar showing the corresponding year (2000-2018). 'r' is Pearson's correlation coefficient.

We also find that cold temperature has an important limitation on seasonal GPP at US-NR1. The seasonal cycle of GPP shows peak productivity in early summer (~June) and falling to near-zero values by early winter (November), continuing through late winter (February-March). Comparison of monthly GPP and minimum, maximum and mean monthly temperature shows an initiation of photosynthesis at monthly maximum temperature above 0 °C (Fig. 3a) and monthly minimum temperature above -5 °C (Fig. 3b). The strong dependence of monthly GPP on temperature is consistent with previous findings that temperature is an important driver of spring onset and seasonal variability of GPP in evergreen forests (e.g., Pierrat et al., 2021; Parazoo et al., 2018; Euskirchen et al., 2014; Arneth et al., 2006). As temperature falls in winter dormant plants, productivity becomes negligible. Productivity is triggered again in spring when sufficient radiation is available for absorption by green needles, and air temperature becomes warm enough to thaw stems, trigger xylem flow and promote access to soil moisture (e.g., Pierrat et al., 2021; Bowling et al., 2018; Ishida et al., 2001). Due to this observed dependence of GPP on temperature at US-NR1, we focus our analysis specifically on spring GPP, where we hypothesize that cold temperature is the dominant control on spring GPP variability.

https://doi.org/10.5194/bg-2021-152
Preprint. Discussion started: 17 June 2021

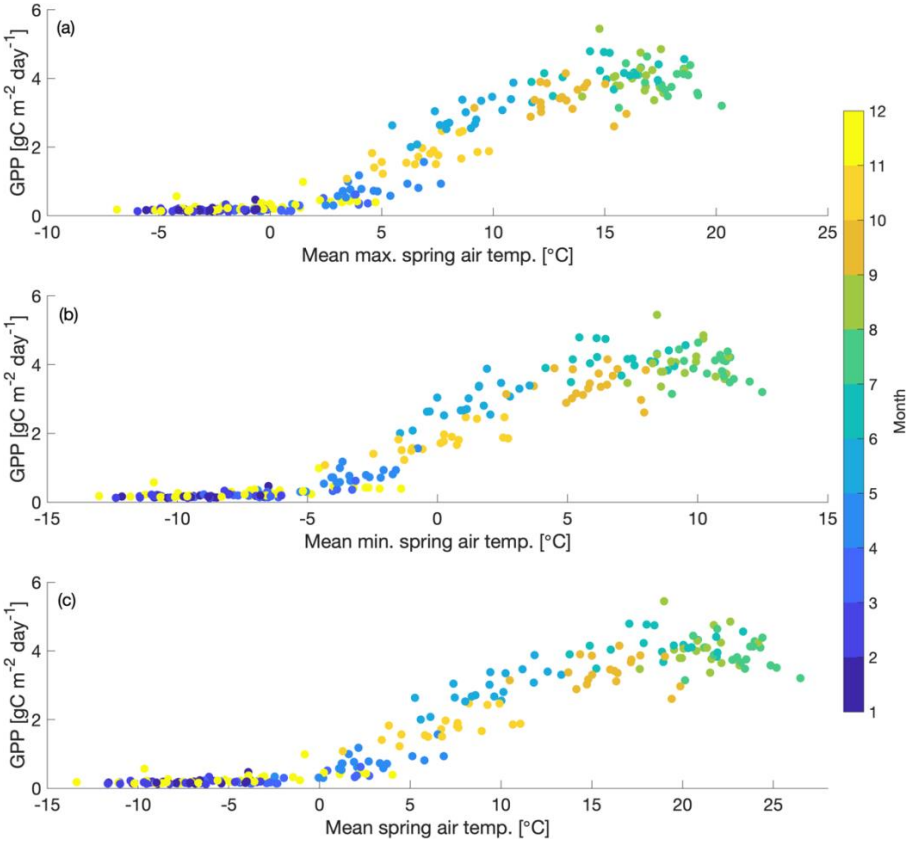

Figure 3. Scatter plot of mean monthly GPP vs. a.) mean maximum air temperature, b.) mean minimum air temperature and c.) mean average air temperature for 2000-2018. Dots are colored with the corresponding month.

In the baseline version of CARDAMOM, seasonal GPP in DALEC2 is limited primarily by incoming shortwave radiation. This light-focused limitation works well for deciduous forests where spring temperature and sunlight are correlated, as well as high latitude regions where sunlight is limited. However, for reasons discussed above, this method fails in evergreen forests such as Niwot Ridge whose green canopies are exposed to high sunlight and below-freezing temperature in spring. As such, we implement a cold temperature scaling factor (g) in DALEC2 (1), to act as a thermostat that regulates evergreen needleleaf carbon uptake phenology. This scaling factor is developed by analyzing the relationship between monthly minimum & maximum temperature with tower-derived monthly GPP, where

$$If: T_{min}(t) < T_0 : g = 0 \quad (1)$$

$$If : T_{min}(t) > T_g : g = 1$$

$$Else: g(t) = \frac{(T_{min}(t) - T_0)}{(T_g - T_0)}$$

$$\mathrm{GPP_{cold}(t)} = \mathrm{GPP(t)} * \mathrm{g(t)} \quad (2)$$

https://doi.org/10.5194/bg-2021-152
Preprint. Discussion started: 17 June 2021

where GPP(t) is the nominal ACM-based DALEC2 GPP estimate (see section 2.3) and GPP_{cold} is the corresponding cold temperature GPP estimate. The temperature thresholds for photosynthesis shutdown (referred to as T_0) and initiation (referred to as T_g) are added as model parameters in DALEC, bringing the total number of parameters to 35. These 35 DALEC parameters are simultaneously optimized in CARDAMOM. The CARDAMOM Bayesian-inference probability distributions (see Appendix A) for the T_0 (-7.1 ± 1.1 °C) and T_g (6.0 ± 2.6 °C) parameters used to define the cold temperature limitation are plotted in Fig S3. We refer to the cold temperature constrained version of DALEC2 (within CARDAMOM) as DALEC2cold.

The baseline (DALEC2) and cold temperature (DALEC2cold) versions of the model are run for the 2000-2018 period using tower observed, gap-filled, monthly meteorological (MET) drivers (including minimum and maximum temperature, shortwave radiation, vapor pressure deficit, and precipitation). We conduct four experiments, summarized in Table 1: experiments using DALEC2 and DALEC2cold within CARDAMOM, where 19 years of GPP data are assimilated (referred to as CARD and CARDcold), and a corresponding pair of experiments where only the first decade of data (2000-2009) is assimilated (referred to as CARD-Half and CARDcold-Half) and the second decade of data (2010-2019) is withheld for validation, as a train-test scenario. All months of GPP data are assimilated into the model, however our analysis focuses on the constraints on spring (March-May) GPP. These four experiments serve to evaluate the sensitivity of modelled GPP at Niwot Ridge to cold temperature limitation, parameter optimization, and data assimilation. Specifically, the objective of experiments "CARD" and "CARDcold" is to determine whether the cold temperature scaling factor improves the representation of spring GPP variability across the 2000-2018 period; the objective of experiments "CARD-Half" and "CARDcold-Half" is to cross-validate the predictive skill of CARDcold by assessing whether the addition of a cold temperature scaling factor, informed by a subset of GPP data, can improve prediction of a withheld subset of GPP data.

Table 1. Summary of CARDAMOM modeling experiments to determine sensitivity of seasonal and interannual spring GPP variability to cold temperature limitation (CARD vs CARDCold) and ability to perform outside training window (Half).

Experiment Name	Met. Drivers	Time Period	GPP assimilation	Time period considered in assimilation	Uncertainties in GPP	Cold Temp. Limitation
CARD	yes	2000-2018	yes	2000-2018	20%	No
CARD-Half	yes	2000-2018	yes	2000-2009	20%	No
CARDCold	yes	2000-2018	yes	2000-2018	20%	Yes
CARDCold-Half	yes	2000-2018	yes	2000-2009	20%	Yes

https://doi.org/10.5194/bg-2021-152
Preprint. Discussion started: 17 June 2021


Biogeosciences Discussions Open Access EGU

2.5. Comparison to Terrestrial Biosphere Model Ensemble

A recent model intercomparison study provides an ideal benchmark for evaluating CARDAMOM simulations (section 2.4). Parazoo et al. (2020) conducted an experiment in which an ensemble of state-of-the-art terrestrial biosphere models (TBMs) were forced by the same observed meteorology at Niwot Ridge from 2000-2018, but with differences in spin-up, land surface characteristics, and parameter tuning. The TBMs are designed to simulate the exchanges of carbon, water, and energy between the biosphere and atmosphere, from global to local scales depending on inputs from meteorological forcing, soil texture, and plant functional type. The experiment is designed primarily to evaluate simulations of solar induced fluorescence (SIF) and GPP, the latter of which we focus on here. We refer the reader to Parazoo et al. (2020) for a more complete description of models, within-model experiments, and between-model differences.

The most important model differences worth noting here include the representation of stomatal-conductance, canopy absorption of incoming radiation, and limiting factors for photosynthesis. We analyze a subset of the models which were run for multiple years, including SiB3 and SiB4 (Simple Biosphere model versions 3 and 4, respectively), ORCHIDEE (Organizing Carbon and Hydrology in Dynamic Ecoystems), BEPS (Boreal Ecosystems Productivity Simulator), and CLM4.5 and CLM5.0 (Community Land Model Versions 4.5 and 5.0, respectively). We also analyze within-model experiments in SiB3 and ORCHIDEE to isolate effects related to prescription of leaf area index (LAI; monthly varying in SiB3-exp1, fixed at 4.0 m^2/m^2 in SiB3-exp2), temperature and water stress (ORCHIDEE-exp1 includes temperature stress; ORCHIDEE-exp2 accounts for temperature and water stress), and data assimilation (ORCHIDEE-exp3, in which a subset of model parameters controlling photosynthesis and phenology are optimized against global OCO-2 SIF data, Bacour et al., 2019). Finally, we note that not all model simulations span the entire observed record (2000-2018). While our analysis focuses on the long term record from 2000-2018, we provide multiple comparison to ensure consistency of time period: (1) IAV from 2001-2018 for SiB3, SiB4, ORCHIDEE, and CLM4.5; (2) IAV from 2012-2018 for SiB3, SiB4, ORCHIDEE, CLM4.5, and CLM5.0, (3) Seasonal variability from 2015-2018 for all models. We refer to the ensemble of models and within model experiments collectively as TBM-MIP.

3. Results & Discussion

3.1. Evaluation of CARDAMOM 2000–2018 GPP

When the 19 years of tower-derived GPP data are assimilated into both versions of the model, the mean seasonal cycle is accurately replicated (Fig. 4). The Pearson's r values for CARD (Fig. 4a) and CARDcold (Fig. 4b) are almost equal (r = 1.0 and 0.99) with minimal increases in root mean square error (RMSE) and mean bias error (MBE) for CARDcold (RMSE = 0.24 g C m^{-2} day^{-1} and 0.23 g C m^{-2} day^{-1}, MBE = 0.06 g C m^{-2} day^{-1} and 0.19 g C m^{-2} day^{-1} for CARD and CARDcold, respectively). Assimilating only the first decade of GPP data (Half experiments) does not drastically alter model performance (Fig. S4), with only slight changes in RMSE and MBE

https://doi.org/10.5194/bg-2021-152
Preprint. Discussion started: 17 June 2021

(ΔRMSE = 0.008 g C m^{-2} day^{-1}, ΔMBE = 0.03 g C m^{-2} day^{-1} for CARD-Half, ΔRMSE = -0.003 g C m^{-2} day^{-1}, ΔMBE = 0.02 g C m^{-2} day^{-1} for CARDcold-Half).

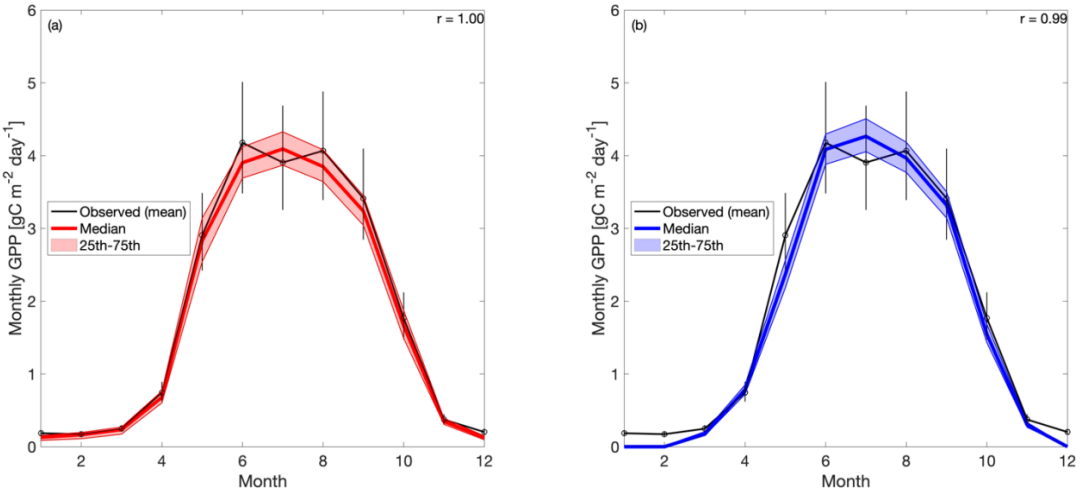

Figure 4. Tower-derived average monthly GPP (black line) and modeled GPP seasonal cycles at US-NR1, averaged for 2000-2018, for a.) CARD and b.) CARDcold experiments. The half-assimilation experiments (CARD-Half and CARDcold-Half) can be found in the supplement (Fig S4). Model outputs include the median value of each experiment (bold color line) with the 25th-75th percentiles of the ensembles (shaded area). The median is plotted instead of the mean to avoid impact of outlier ensemble members (N = 4000). Error bars = tower-derived GPP multiplied/divided by exp(sqrt(log(2)^2*n)/n), n=# of years in average (n = 19). 'r' is the Pearson's coefficient.

The cold experiments exhibit an improved fit to the observed IAV in spring productivity (Fig. 5), relative to CARD, (r = 0.47, std = 0.03 g C m^{-2} day^{-1} for CARD; r = 0.88, std = 0.27 g C m^{-2} day^{-1} for CARDcold). CARDcold also has slightly reduced RMSE (-0.01 g C m^{-2} day^{-1}) and larger MBE (0.13 g C m^{-2} day^{-1}). Similar to the seasonal cycle analysis, the assimilation of only the first decade of GPP data (Half experiments) has minimal impact on model performance (ΔRMSE = 0.007 g C m^{-2} day^{-1}, ΔMBE = 0.06 g C m^{-2} day^{-1} for CARD-Half, and ΔRMSE = 0.02 g C m^{-2} day^{-1}, ΔMBE = 0.02 g C m^{-2} day^{-1} for CARDcold-Half). We find less agreement between modelled and tower-derived GPP IAV in summer for both CARD and CARDcold (CARD r = 0.32, std = 0.11 g C m^{-2} day^{-1}; CARDcold r = 0.05, std = 0.10 g C m^{-2} day^{-1}; Fig. S5). While there is little variation in RMSE between the half and full-assimilation experiments, RMSE is larger for summer than spring GPP (average RMSE = 0.23 g C m^{-2} day^{-1} for spring model outputs, average RMSE = 0.35 g C m^{-2} day^{-1} for summer model outputs). Model agreement is further reduced when considering annual average GPP (Fig. S6, Table S2). Although the cold temperature limitation improves IAV slightly, it is still small compared to observed variability (std = 0.14 g C m^{-2} day^{-1}). Correlations to tower-derived GPP at the annual scale are small for both CARD and CARDcold (r = 0.19 and r = 0.22, Fig. S6a-b). Overall, the cold temperature limitation substantially improves agreement between the model and tower-derived spring GPP, with slight reductions in performance for summer and annual GPP.

https://doi.org/10.5194/bg-2021-152
Preprint. Discussion started: 17 June 2021

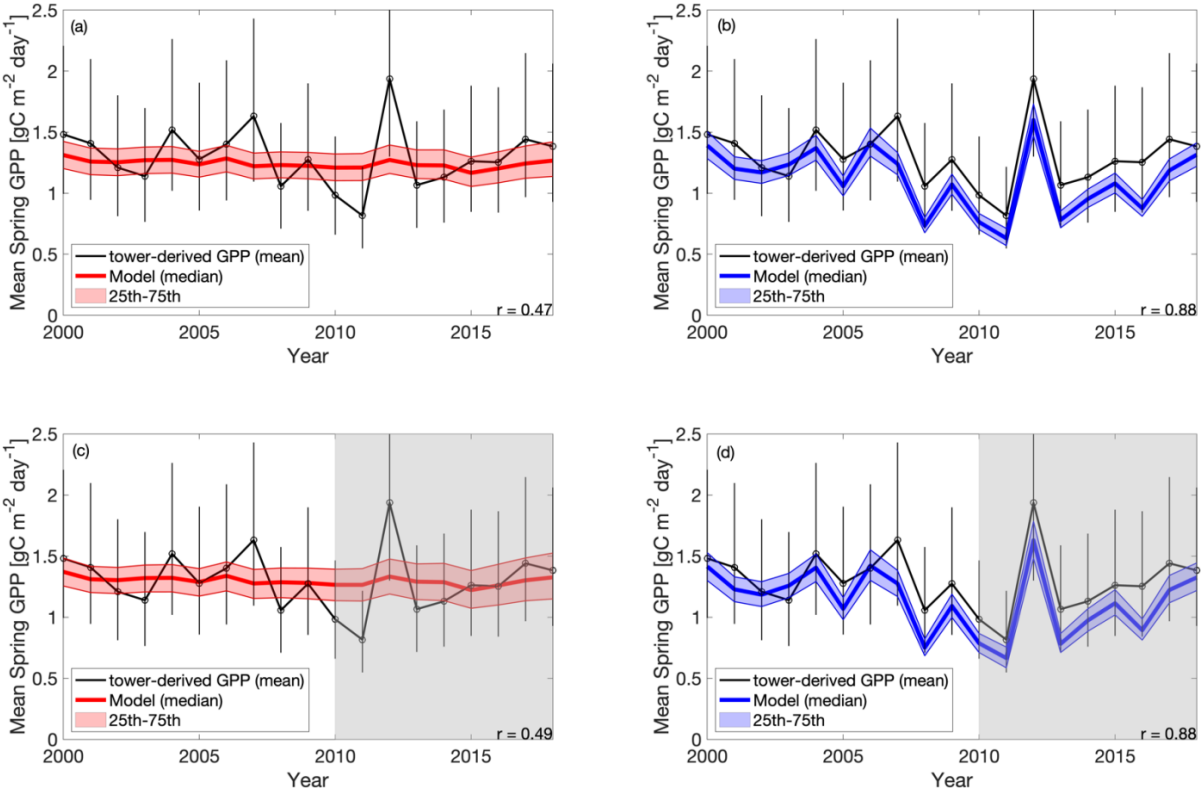

Figure 5. Tower-derived (black line) mean spring (March-May) GPP with model interquartile range (shaded area) and median (bold color line) spring GPP outputs for a.) CARD, b.) CARDcold, c.) CARD-Half, and d.) CARDcold-Half experiments. The grey regions indicate no data assimilation (i.e. testing window). Model experiments are the same as in Figure 4. Uncertainty = exp(sqrt(log(2)^2*n)/n), n=# of months in average (n = 3).

The standard deviation in tower-derived mean spring GPP (March-May) is approximately 0.25 g C m^{-2} day^{-1}. The addition of the cold temperature limitation improves the model's ability to match the IAV of mean spring GPP (Fig. 6a-b). An examination of all modeled scenarios for CARD and CARDcold (i.e. all 4000 DALEC2 simulations), shows that the cold temperature limitation produces spring IAV values much closer to what is observed in the tower-derived GPP data. Only 0.3% of CARD ensembles produces mean spring IAV values within 20% of the tower-derived spring GPP standard deviation (0.25 ± 0.05 g C m^{-2} day^{-1}), whereas 69% of CARDcold ensembles have standard deviation values within the same range. Interestingly, assimilating only the first ten years of GPP data (Half experiments, Fig. 6b) slightly increases the number of ensemble members with standard deviations within the mentioned range for both CARD-Half (2.4%) and CARDcold-Half (70%). It is promising to see that despite not assimilating the 2010-2018 GPP data into the model, CARDcold-Half is still able to match average spring IAV of the full data record.

We also consider the IAV in spring GPP for just the second half of the data record (2010-2018). IAV of tower-derived spring GPP increases slightly in 2010-2018 (0.32 g C m^{-2} day^{-1}). Once again, the cold temperature limitation enables CARDAMOM to match spring GPP IAV (Fig. 6c-d). 0.03% of CARD ensembles produce mean

https://doi.org/10.5194/bg-2021-152
Preprint. Discussion started: 17 June 2021

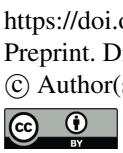

spring IAV values within 20% of the tower-derived spring GPP standard deviation for the 2010-2018 period (0.32 ± 0.06 g C m^{-2} day^{-1}), whereas 76% of CARDcold ensembles have standard deviation values within the same range. For the Half experiments, 0.6% of CARD and 75% of CARDcold ensembles have IAV values within 20% of the standard deviation for 2010-2018. Overall, CARDcold produces a less biased distribution of IAV values (relative to both assimilated and withheld observations), whereas CARD is more skewed towards smaller IAVs, which indicates that the cold temperature limitation enables a mechanistic and statistical improvement in capturing the interannual variability of spring GPP.

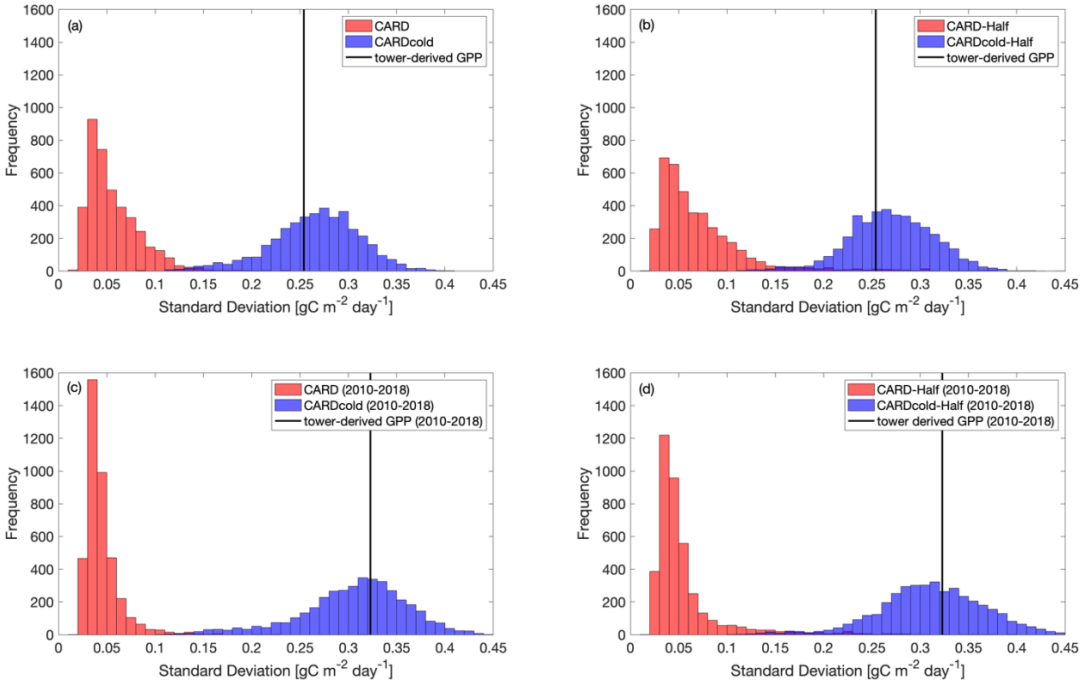

Figure 6. Histograms comparing standard deviation in mean spring GPP across all ensembles (N=4000) for CARD (red bars) and CARDcold (blue bars) experiments with a.) full assimilation, b.) half assimilation, c.) full assimilation for the second decade (2010-2018), and d.) half assimilation for the second decade (2010-2018). Black line indicates standard deviation in tower-derived mean spring GPP (std = 0.25 gC m^{-2} day^{-1} for full period, std = 0.32 gC m^{-2} day^{-1} for 2010-2018).

3.2. Temperature controls on springtime GPP

The added value of the DALEC2 cold temperature limitation for modelling mean spring (March-May) GPP is logically due to large fluctuations in spring temperature at Niwot Ridge. The cold temperature limitation allows DALEC2-CARDAMOM to match the IAV of spring tower-derived GPP closely. Furthermore, the cold temperature limitation enables the model to match tower spring IAV in the second half of the time period (2010-2018) when only the first ten years of GPP data are assimilated (2000-2009). This indicates that the cold temperature limitation is able to estimate spring GPP outside of its training window and could be useful at other sites where data availability

https://doi.org/10.5194/bg-2021-152
Preprint. Discussion started: 17 June 2021

is limited. Future work will include evaluating the cold temperature limitation at other sites to ensure that it is applicable beyond Niwot Ridge, for example using forecast skill metrics proposed by Famiglietti et al. (2020).

Temperature-induced spring onset of GPP is driven by two general processes (1) initiation of bud burst and leaf expansion leading to increasing LAI, and/or (2) initiation of photosynthetic activity (photosynthetic efficiency i.e. GPP per unit LAI) due to temperature-induced changes in plant hydraulics (Ishida et al., 2001; Pierrat et al., 2021) or kinetics of the photosynthetic machinery (e.g. Medlyn et al., 2002). In-situ LAI measurements suggest that the LAI at Niwot Ridge is relatively constant across the season, which is somewhat expected given the dominant tree species at the site. Hence, the temperature-induced onset of GPP is likely due to the latter process, increased photosynthetic efficiency, as supported by the measurements (Fig. 2), although small changes in LAI are still feasible given uncertainties in the measurements. The inclusion of the cold-temperature limitation scaling factor in the model, a semi-empirical process, leads to a substantial improvement in model representation of GPP at the site. Further development may look to identify the relative roles of increased LAI and increased photosynthetic efficiency at Niwot Ridge and other evergreen needleleaf sites, as changes in GPP can lead to changes in carbon allocation to LAI, among other plant carbon pools.

With the inclusion of the cold-temperature limitation on GPP and its application in CARDAMOM we provide a data-constrained estimate of the climate-sensitivity of the Niwot Ridge forest to spring temperatures. Posterior estimates indicate that GPP is gradually inhibited below 6.0 °C ± 2.6 °C (T_g) and completely inhibited below -7.1 °C ± 1.1 °C (T_0). The gradual limitation of GPP by temperature has been observed on hourly and daily timescales in other cold-weather ecosystems, such as Alaskan conifers (Parazoo et al., 2018) and Canadian spruce e(Pierret et al., 2020). This has been connected to the triggering of transpiration and water flow from xylem into leaves (Ishida et al., 2001). However, both biotic (carotenoid/chlorophyll ratios) and abiotic (canopy airspace) factors together regulate GPP response to meteorological forcings, and further process-oriented investigations are required to resolve the emergent response of GPP to temperature. For now, this is a useful metric for climate-sensitivity of spring GPP, at least in the absence of long-term adaptations. Furthermore, over the 19 year observation period investigated here the use of a temporally constant T_0 and T_g yields significantly improved suggesting that much of the variability can be attributed to climate-driven changes, not interannual variation in vegetation parameters. As temperature continues to increase due to climate change (particularly in the early growing season), productivity at US-NR1 could increase as a result and therefore increase carbon uptake, with productivity peaking earlier in the year (e.g., Xu et al., 2016). However, these spring gains in GPP have been shown to not offset the losses of carbon due to summer droughts (e.g., Buermann et al., 2013; Knowles et al., 2018). It is also unclear how the long-term stress of increased temperature could affect forest productivity directly.

This study focuses on the relationship between temperature and GPP and its usefulness on model predictions of spring GPP, but an important component that cannot be ignored is the confounding effect of water availability on GPP. Future changes in winter precipitation are more uncertain, therefore limiting our ability to analyze how precipitation changes will alter future productivity. While precipitation observations are analyzed to discern any major connections between GPP and meteorological controls, an analysis of how precipitation affects model predictability is not included in this study. The combined results, including the cold temperature limitation

https://doi.org/10.5194/bg-2021-152
Preprint. Discussion started: 17 June 2021

and train-test data assimilation experiments, suggest that other factors besides spring temperature, most notably winter and summer precipitation (Fig. 2) and resulting soil water limitation, also have important impacts on summer GPP. We therefore highlight the need to jointly resolve spring-time temperature limitations in conjunction with water stress limitations in future efforts to understand the integrated role of environmental forcings on interannual GPP variability. Furthermore, this analysis does not consider how winter precipitation as snowfall versus rainfall affected productivity, or how resulting changes to winter snowpack could alter productivity long-term. Since annual average GPP appears to be more dependent on winter precipitation/snowpack, future work will include improving model predictability of late season productivity and quantifying temperature-water effects on carbon uptake. The definition of the seasons could also alter the connections drawn between seasonal temperature, precipitation and productivity.

3.3. Model intercomparison and implications for GPP models

Here, we evaluate DALEC2-CARDAMOM against mean spring GPP estimates from TBM-MIP models (Section 2.5 and Parazoo et al. 2020). It is important to remind the reader that the CARDAMOM runs have a significant advantage over the TBM-MIP models in this analysis, as CARDAMOM is trained on US-NR1 GPP data. While TBM-MIP models use tower-observed meteorological inputs, prescribe tower-specific and time-invariant structural properties such as LAI observed at US-NR1 (SiB3-exp2 & CLM4.5), and use data assimilation of global remote sensing data to constrain globally-representative plant functional types (ORCHIDEE-exp3), they are not directly constrained by time-varying carbon fluxes at the tower. As such, we emphasize that our model comparison is not a competition, but rather an attempt to discern common environmental controls in model performance of simulating the magnitude and seasonal-to-interannual variability of spring GPP at an evergreen needleleaf site.

There is a wide range in performance of TBM-MIPs in representing the magnitude and IAV or tower-derived spring GPP (Figure 7a). Pearson's r correlations range from 0.25 to 0.82 (mean r = 0.6, Table 2) from 2001-2018, with the same models showing slightly improved performance over the second decade (mean r = 0.73 from 2012-2018). ORCHIDEE-exp1 and CLM4.5 show consistently high performance over all three periods analyzed, with CLM5.0 excelling from 2012-2018, and BEPS from 2015-2018 (Table S1). CLM4.5 also shows smallest mean bias of the TBM-MIP models (RMSE ~ 0.35), and high agreement in the magnitude of spring GPP variability (1-sigma standard deviation = 0.21 g C m^{-2} day^{-1} for CLM4.5, vs 0.25 g C m^{-2} day^{-1} observed). While acknowledging the advantage of data assimilation, it is promising to see that CARDAMOM (with the addition of the cold temperature limitation) is able to perform comparably to the TBM-MIP models. In particular, CARDcold is well correlated in the direction (r = 0.88) and magnitude (1-sigma ~0.26) of interannual variability, as well as overall magnitude of spring GPP (low RMSE and MBE).

The range of performance across within-model experiments reveals important processes, and uncertainty of process representation, in driving the magnitude and variability of spring GPP. For example, the ORCHIDEE data assimilation experiment (exp3) shows consistently and substantially lower overall correlation (e.g., r = 0.59 from 2001-2018) than corresponding free running experiments (exp 1 and 2, r = 0.78-0.82), but has reduced RMSE and MBE (RMSE = 0.63 g C m^{-2} day^{-1} vs 1-1.14 g C m^{-2} day^{-1}). Likewise in SiB3, prescribing an empirically-based but

https://doi.org/10.5194/bg-2021-152
Preprint. Discussion started: 17 June 2021

fixed-in-time LAI (exp2) reduces mean bias, but degrades variability (r = 0.25) compared to time-variable LAI (exp1) prescribed from satellite data (r = 0.50).

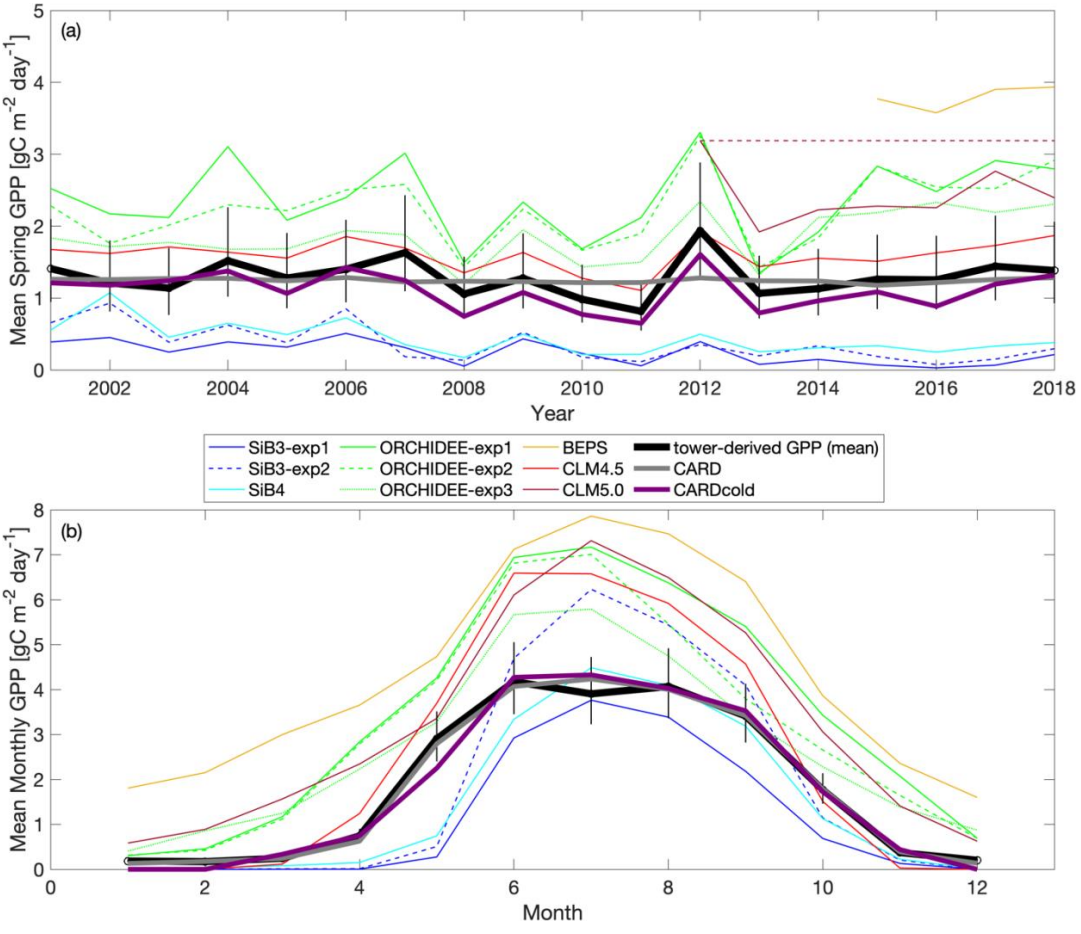

Figure 7. Comparison of TBM-MIP models to CARD and CARDcold experiments for a.) mean spring GPP and b.) monthly GPP. Note that fill values are ignored when calculating mean annual values for TBM-MIP experiments. Uncertainty = exp(sqrt(log(2)^2*n)/n), where n = # years in average (n = 19).

There is also large variability in the modeled seasonal cycle (Fig. 7b) and mean annual GPP (Fig. S7). For mean annual GPP estimates, Pearson's r values are reduced for all models (Table S2). Once again, ORCHIDEE-exp2 and ORCHIDEE-exp3 stand out with some of the higher correlations (r = 0.60 and r = 0.64) and p-values below 5% significance level. Furthermore, ORCHIDEE-exp3 (temperature stress with SIF data assimilation) has the lowest RMSE and MBE of the model set. SiB3-exp2 (fixed LAI) has a standard deviation closest to "observations" (0.14 gC m^{-2} day^{-1}), and the smallest RMSE and MBE of the TBM models.

https://doi.org/10.5194/bg-2021-152
Preprint. Discussion started: 17 June 2021

Most TBM-MIP models capture the shape of the seasonal cycle at Niwot Ridge. For the 2015-2018 period, all models have Pearson's r values larger than 0.91, with p-values much smaller than a 5% significance level (Table S3). With the help of data assimilation, CARDcold accurately captures the seasonal cycle at Niwot Ridge with reduced error (RMSE = 0.22 g C m^{-2} day^{-1}, MBE = 0.07 g C m^{-2} day^{-1}), and data assimilation experiments in ORCHIDEE-exp3 show reduced bias relative to free running experiments. The cold temperature limitation has little impact on the modeled mean seasonal cycle or mean annual GPP estimates in CARDAMOM, and appears to be most valuable for improving spring GPP variability.

Table 2. Pearson's linear r, R-squared, p-value, standard deviation, root mean square error (RMSE), and mean bias error (MBE) for TBM-MIP and all CARDAMOM experiments to Niwot Ridge tower-derived mean spring (March-May) GPP. Open values reflect statistics for the 2001-2018 period, while values in parentheses represent the 2012-2018 period. All relevant statistics are calculated at 5% significance level. *BEPs statistics are not included in this table as this model only has GPP estimates for 2015-2018.

model	r-value	R-squared	p-value (α = 0.05)	RMSE (gC m^{-2} d^{-1})	MBE (gC m^{-2} d^{-1})	standard deviation (gC m^{-2} d^{-1})
CARD-Half	0.47 (0.55)	0.22 (0.30)	0.05 (0.20)	0.24 (0.26)	-0.005 (0.06)	0.03 (0.04)
CARD	0.45 (0.57)	0.20 (0.33)	0.06 (0.18)	0.24 (0.28)	0.05 (0.12)	0.03 (0.04)
CARDcold-Half	0.88 (0.93)	0.77 (0.86)	0.00 (0.002)	0.21 (0.24)	0.17 (0.22)	0.26 (0.29)
CARDcold	0.87 (0.93)	0.76 (0.87)	0.00 (0.00)	0.23 (0.26)	0.20 (0.24)	0.26 (0.28)
SiB3-exp1	0.50 (0.81)	0.25 (0.66)	0.04 (0.03)	1.07 (1.23)	1.04 (1.21)	0.16 (0.13)
SiB3-exp2	0.25 (0.41)	0.06 (0.17)	0.32 (0.36)	0.97 (1.15)	0.92 (1.13)	0.26 (0.10)
SiB4	0.34 (0.91)	0.12 (0.83)	0.16 (0.00)	0.90 (1.04)	0.86 (1.02)	0.22 (0.09)
ORCHIDEE-exp1	0.82 (0.82)	0.68 (0.67)	0.00 (0.02)	1.14 (1.24)	-1.08 (-1.16)	0.56 (0.67)
ORCHIDEE-exp2	0.78 (0.79)	0.61 (0.63)	0.00 (0.03)	1.00 (1.20)	-0.95 (-1.12)	0.51 (0.64)
ORCHIDEE-exp3	0.59 (0.55)	0.35 (0.31)	0.01 (0.20)	0.63 (0.81)	-0.57 (-0.76)	0.35 (0.36)
BEPS*	X	X	X	X	X	X
CLM4.5	0.82 (0.85)	0.68 (0.73)	0.00 (0.01)	0.34 (0.35)	-0.31 (-0.31)	0.21 (0.18)
CLM5.0	(0.96)	(0.92)	(0.00)	(1.09)	(-1.08)	(0.42)

In summary, TBM-MIP experiments reveal several key factors that can improve or degrade estimates of spring GPP at Niwot Ridge. For example, adapting model parameters to needleleaf species based on hand-tuning to tower data and formal data assimilation methods (CLM4.5 and ORCHIDEE-exp3, respectively) improves the overall magnitude of spring GPP. Likewise, prescribing LAI to a constant value of 4.0 m^2/m^2 based on tower measurements (SiB3-exp1) improves spring GPP magnitude, while prescribing time variable LAI based on MODIS data improves year-to-year variability (SiB3-exp2). SIB4, which has prognostic rather than prescribed phenology, represents a compromise in magnitude and variability when looking at the entire record (2001-2018), but is one of the top performers across all TBM-MIP models over the most recent period (2012-2018).

We did not directly consider changes in canopy structural or biophysical characteristics in our CARDAMOM experiments. In CARDAMOM, LAI is a prognostic quantity (a function of foliar C and leaf carbon mass per area). In the absence of LAI observational constraints, CARDAMOM LAI is indirectly informed by the

https://doi.org/10.5194/bg-2021-152
Preprint. Discussion started: 17 June 2021

448 constraints of time-varying GPP on DALEC2 parameters (see section 2.3). Our results suggest that additional
449 improvements are possible with careful consideration of in-situ measured vegetation parameters.
450 TBM-MIP experiments also offer insight on important environmental controls and process representation.
451 Air temperature is an effective constraint of spring GPP onset (CLM4.5, ORCHIDEE-exp1), but which can be
452 degraded when large scale data assimilation does not account for local- to regional- vegetation characteristics in
453 parameter optimization (e.g., ORCHIDEE-exp3). Water availability appears to be a secondary but still important
454 driver of spring GPP. While acknowledging the numerous differences between CLM4.5 and CLM5.0, we find it
455 important to note that plant hydraulic water stress (CLM5.0) shows improved IAV performance (high correlation
456 and reduced error) over simplified soil moisture stress functions (CLM4.5). This result further supports efforts to
457 closely analyze seasonal GPP to locate different environmental controls for future model improvements.
458 While further experiments are needed, these results demonstrate the value of (1) site-level data assimilation
459 for local scale prediction of GPP magnitude and variability, (2) global data assimilation for reducing magnitude
460 biases, and (3) process formulation for accounting for sensitivity to temperature limitation and water stress. Overall,
461 these results are encouraging for model-data fusion systems which have developed the capacity to bring together
462 temporally and spatially resolved functional and structural vegetation components such as LAI, SIF, soil organic
463 matter, and above- and below-ground biomass (e.g., Bacour et al., 2019; Smith et al., 2020; Bloom et al., 2020).
464 Joint assimilation of these datasets, coupled with observed meteorological forcing, has potential to introduce more
465 emergent constraints of vegetation change with respect to environmental change, thus improving overall estimates of
466 productivity. Future work will assess the joint impact of SIF, ET, LAI, and biomass data as effective constraints on
467 light use and water use efficiency (Smith et al., 2019), which is expected to improve the ability of CARDAMOM to
468 use light with respect to increasing biomass subject to longer growing seasons and heat and water stress.

469 **4. Conclusions**

470 Despite mechanistic advances in ecosystem modeling, it is still a challenge to simulate temporal variations
471 in GPP. In an attempt to dissect the environmental controls on GPP in an evergreen needleleaf ecosystem, we
472 analyzed the impact of temperature on spring (March-May) productivity by implementing a cold temperature GPP
473 limitation within a model-data fusion system (DALEC2-CARDAMOM). The cold weather GPP limitation allows
474 for improved model estimates of productivity at Niwot Ridge, specifically CARDAMOM's ability to match the
475 interannual variability observed in tower-derived mean spring GPP. Furthermore, CARDAMOM is able to match
476 spring interannual variability between model and tower data outside of the training period. When compared to
477 TBM-MIP models, controls that appear to impact model performance include the inclusion of water stress (e.g. soil
478 moisture) and vegetation parameters (e.g. prescription of LAI). The fact that the cold temperature limitation does not
479 improve CARDAMOM's annual GPP estimates suggests that other controls (i.e. winter precipitation) drive GPP
480 variability in other parts of the year, most likely summer (June-September). The cold temperature limitation may
481 prove useful in understanding future changes in spring productivity due to changes in temperature in important
482 ecosystems, such as the Western U.S.

https://doi.org/10.5194/bg-2021-152
Preprint. Discussion started: 17 June 2021

Appendices

Appendix A: Model-Data Fusion Methodology

The DALEC2 model parameter values and state variable initial conditions (henceforth $\boldsymbol{x}$) are optimized using a Bayesian inference approach, where the posterior probability distribution of $\boldsymbol{x}$ given observations O, p(x|O), can be expressed as

$$p(\boldsymbol{x}|\boldsymbol{o}) \propto p(\boldsymbol{x})L(\boldsymbol{x}|\boldsymbol{O}) \quad \text{(A1)}$$

Where p($\boldsymbol{x}$) is the prior probability distribution of $\boldsymbol{x}$, and L($\boldsymbol{x}$|O) is the likelihood of the DALEC parameters and initial conditions given observations **O**. We define the likelihood function as

$$L(\boldsymbol{x}|\boldsymbol{o}) = \mathrm{e}^{-\frac{1}{2}\sum i\left(\frac{m_i(x)-o_i}{\sigma}\right)^2} + \mathrm{e}^{-\frac{1}{2}\sum a\left(\frac{m'_a(x)-o'_a}{\sigma'}\right)^2}, \quad \text{(A2)}$$

where for monthly timestep i, $m_i(\boldsymbol{x})$ and o_i represent monthly modelled GPP (based on parameters **x**) and flux-tower GPP observation, respectively. Following model-data fusion efforts with a spectrum of temporal modes of variability (Desai 2010, Quetin et al., 2020 and Bloom et al., 2020), we extend the cost function to include mean annual model and tower-derived GPP, $m_a(\boldsymbol{x})$ and o_a respectively) for year = a, which allows the GPP cost function to be sensitive to both seasonal and inter-annual components of the flux tower GPP signal. We log-transform modelled and tower-derived GPP values (as done in Bloom & Williams, 2015 and Bloom et al., 2016), which is preferable for characterize model-data residuals between strictly positive quantities (such as GPP). For lack of better uncertainty estimates on monthly and annual flux tower GPP accuracy—including lack of knowledge on GPP error characteristics at monthly timescales, error covariance between individual GPP estimates, model structural error impacts on GPP —we conservatively prescribed uncertainty factor of $\sigma = 2$ for monthly values (roughly ~75%), and σ' = 1.2 (~18%) for annual values; in general we found that these values led to robust agreements between flux tower and DALEC2 GPP variability (model-data mismatch metrics are reported in section 3 of the manuscript).

For all model experiments, we sample the probability of $p(\boldsymbol{x}|\boldsymbol{o})$, the posterior probability distribution of initial conditions $\boldsymbol{x}$ given observations o, we use four Metropolis-Hastings Markov Chain Monte Carlo (MHMCMC; Haarrio et al. 2001) for 10^8 iterations; we subsample 1000 parameter vectors $\boldsymbol{x}$, from the latter 50% of each chain (in total 1000 samples x 4 chains = 4000 samples). We test for convergence in the MHMCMC estimates of $\boldsymbol{x}$ using a the Gelman-Rubin convergence diagnostic to measure convergence between the four chains.

Data Availability

The Ameriflux US-NR1 data was obtained from: https://ameriflux.lbl.gov/sites/siteinfo/US-NR1 (Blanken et al., 2020). The US-NR1 data used in this study, as well as the CARDAMOM and TBM-MIP outputs are publicly available and provided in .nc file format at http://doi.org/10.5281/zenodo.4928097 .

https://doi.org/10.5194/bg-2021-152
Preprint. Discussion started: 17 June 2021

Code Availability

The CARDAMOM code used in this study is available here: https://github.com/CARDAMOM-framework/CARDAMOM_v2.2

Author Contributions

SGS, NCP and AAB designed and performed the research. AJN, BR, CB, FM, IB, YZ, BQ, and MS contributed model simulations. DRB, SPB, and PDB contributed observational data. All authors contributed to the writing of the paper.

Supplement

Competing Interests

The authors declare that they have no conflict of interest.

Acknowledgements

The US-NR1 AmeriFlux site has been supported by the U.S. DOE, Office of Science through the AmeriFlux Management Project (AMP) at Lawrence Berkeley National Laboratory under Award Number 7094866. A portion of this research was carried out at the Jet Propulsion Laboratory, California Institute of Technology, under contract with NASA. Funding from the NASA Earth Science Division Arctic Boreal Vulnerability Experiment (ABoVE) is acknowledged. We acknowledge the MEASUREs program. DRB and BMR were supported by the NASA CMS (NNX16AP33G) and the NSF Macrosystems Biology and NEON-Enabled Science (1926090) Programs. The National Center for Atmospheric Research (NCAR) is sponsored by NSF.

References

Anav, A., Friedlingstein, P., Beer, C., Ciais, P., Harper, A., Jones, C., Murray-Tortarolo, G., Papale, D., Parazoo, N. C., Peylin, P., Piao, S., Sitch, S., Viovy, N., Wiltshire, A., and Zhao, M.: Spatiotemporal patterns of terrestrial gross primary production: A review, 53, 785–818, https://doi.org/10.1002/2015RG000483, 2015.

Anderson-Teixeira, K. J., Delong, J. P., Fox, A. M., Brese, D. A., and Litvak, M. E.: Differential responses of production and respiration to temperature and moisture drive the carbon balance across a climatic gradient in New Mexico: CARBON BALANCE ACROSS NM ELEVATIONAL GRADIENT, 17, 410–424, https://doi.org/10.1111/j.1365-2486.2010.02269.x, 2010.

Arneth, A., Lloyd, J., Shibistova, O., Sogachev, A., and Kolle, O.: Spring in the boreal environment: observations on pre- and post-melt energy and CO_2 fluxes in two central Siberian ecosystems, 11, 311–328, 2006.

Bacour, C., Maignan, F., MacBean, N., Porcar-Castell, A., Flexas, J., Frankenberg, C., Peylin, P., Chevallier, F., Vuichard, N., and Bastrikov, V.: Improving Estimates of Gross Primary Productivity by Assimilating Solar-Induced Fluorescence Satellite Retrievals in a Terrestrial Biosphere Model Using a Process-Based SIF Model, 124, 3281–3306, https://doi.org/10.1029/2019JG005040, 2019.

549
550 Baldocchi, D. 'Breathing' of the terrestrial biosphere: lessons learned from a global network of carbon dioxide flux
551 measurement systems, Aust. J. Bot., 56, 1–26, https://doi.org/10.1071/BT07151, 2008.
552 Baldocchi, D., Chu, H., and Reichstein, M.: Inter-annual variability of net and gross ecosystem carbon fluxes: A
553 review, Agricultural and Forest Meteorology, 249, 520–533, https://doi.org/10.1016/j.agrformet.2017.05.015, 2018.
554
555 Beer, C., Reichstein, M., Tomelleri, E., Ciais, P., Jung, M., Carvalhais, N., Rödenbeck, C., Arain, M. A., Baldocchi,
556 D., Bonan, G. B., Bondeau, A., Cescatti, A., Lasslop, G., Lindroth, A., Lomas, M., Luyssaert, S., Margolis, H.,
557 Oleson, K. W., Roupsard, O., Veenendaal, E., Viovy, N., Williams, C., Woodward, F. I., and Papale, D.: Terrestrial
558 Gross Carbon Dioxide Uptake: Global Distribution and Covariation with Climate, 329, 834–838,
559 https://doi.org/10.1126/science.1184984, 2010.
560
561 Blanken, P.D, Monson, R.K., Burns, S.P., Bowling, D.R., Turnipseed, A.A.: Ameriflux US-NR1 Niwot Ridge
562 Forest (LTER NWT1), Ver. 16-5, AmeriFlux AMP, (Dataset). https://doi.org/10.17190/AMF/1246088, 2020.
563
564 Bloom, A. A. and Williams, M.: Constraining ecosystem carbon dynamics in a data-limited world: integrating
565 ecological "common sense" in a model–data fusion framework, 12, 1299–1315, https://doi.org/10.5194/bg-12-1299-
566 2015, 2015.
567
568 Bloom, A. A., Exbrayat, J.-F., Velde, I. R. van der, Feng, L., and Williams, M.: The decadal state of the terrestrial
569 carbon cycle: Global retrievals of terrestrial carbon allocation, pools, and residence times, PNAS, 113, 1285–1290,
570 https://doi.org/10.1073/pnas.1515160113, 2016.
571
572 Bloom, A. A., Bowman, K. W., Liu, J., Konings, A. G., Worden, J. R., Parazoo, N. C., Meyer, V., Reager, J. T.,
573 Worden, H. M., Jiang, Z., Quetin, G. R., Smallman, T. L., Exbrayat, J.-F., Yin, Y., Saatchi, S. S., Williams, M., and
574 Schimel, D. S.: Lagged effects dominate the inter-annual variability of the 2010-2015 tropical carbon balance, 1–49,
575 https://doi.org/10.5194/bg-2019-459, 2020.
576
577 Bowling, D. R., Logan, B. A., Hufkens, K., Aubrecht, D. M., Richardson, A. D., Burns, S. P., Anderegg, W. R. L.,
578 Blanken, P. D., and Eiriksson, D. P.: Limitations to winter and spring photosynthesis of a Rocky Mountain
579 subalpine forest, Agricultural and Forest Meteorology, 252, 241–255,
580 https://doi.org/10.1016/j.agrformet.2018.01.025, 2018.
581
582 Buermann, W., Bikash, P. R., Jung, M., Burn, D. H., and Reichstein, M.: Earlier springs decrease peak summer
583 productivity in North American boreal forests, 8, 024027, https://doi.org/10.1088/1748-9326/8/2/024027, 2013.
584
585 Buermann, W., Forkel, M., O'Sullivan, M., Sitch, S., Friedlingstein, P., Haverd, V., Jain, A. K., Kato, E., Kautz, M.,
586 Lienert, S., Lombardozzi, D., Nabel, J. E. M. S., Tian, H., Wiltshire, A. J., Zhu, D., Smith, W. K., and Richardson,
587 A. D.: Widespread seasonal compensation effects of spring warming on northern plant productivity, 562, 110–114,
588 https://doi.org/10.1038/s41586-018-0555-7, 2018.
589
590 Burns, S., Maclean, G., Blanken, P., Oncley, S., Semmer, S., and Monson, R.: The Niwot Ridge Subalpine Forest
591 US-NR1 AmeriFlux site – Part 1: Data acquisition and site record-keeping, 5, 451–471, https://doi.org/10.5194/gi-5-
592 451-2016, 2016.
593
594 Burns, S. P., Swenson, S. C., Wieder, W. R., Lawrence, D. M., Bonan, G. B., Knowles, J. F., and Blanken, P. D.: A
595 Comparison of the Diel Cycle of Modeled and Measured Latent Heat Flux During the Warm Season in a Colorado
596 Subalpine Forest, 10, 617–651, https://doi.org/10.1002/2017MS001248, 2018.
597
598 Euskirchen, E. S., Carman, T. B., and McGuire, A. D.: Changes in the structure and function of northern Alaskan
599 ecosystems when considering variable leaf-out times across groupings of species in a dynamic vegetation model, 20,
600 963–978, https://doi.org/10.1111/gcb.12392, 2014.
601
602 Exbrayat, J.-F., Bloom, A. A., Falloon, P., Ito, A., Smallman, T. L., and Williams, M.: Reliability ensemble
603 averaging of 21st century projections of terrestrial net primary productivity reduces global and regional
604 uncertainties, Earth Syst. Dynam., 9, 153–165, https://doi.org/10.5194/esd-9-153-2018, 2018.

https://doi.org/10.5194/bg-2021-152
Preprint. Discussion started: 17 June 2021

Famiglietti, C. A., Smallman, T. L., Levine, P. A., Flack-Prain, S., Quetin, G. R., Meyer, V., Parazoo, N. C., Stettz, S. G., Yang, Y., Bonal, D., Bloom, A. A., Williams, M., and Konings, A. G.: Optimal model complexity for terrestrial carbon cycle prediction, Biogeochemistry: Modelling, Terrestrial, https://doi.org/10.5194/bg-2020-478, 2020.

Forkel, M., Carvalhais, N., Rödenbeck, C., Keeling, R., Heimann, M., Thonicke, K., Zaehle, S., and Reichstein, M.: Enhanced seasonal CO2 exchange caused by amplified plant productivity in northern ecosystems, 351, 696–699, https://doi.org/10.1126/science.aac4971, 2016.

Frank, J. M., Massman, W. J., Ewers, B. E., Huckaby, L. S., and Negrón, J. F.: Ecosystem CO2/H2O fluxes are explained by hydraulically limited gas exchange during tree mortality from spruce bark beetles, 119, 1195–1215, https://doi.org/10.1002/2013JG002597, 2014.

Goulden, M. and Bales, R.: California forest die-off linked to multi-year deep soil drying in 2012–2015 drought, Nature Geoscience, 12, 1, https://doi.org/10.1038/s41561-019-0388-5, 2019.

Goulden, M. L., Anderson, R. G., Bales, R. C., Kelly, A. E., Meadows, M., and Winston, G. C.: Evapotranspiration along an elevation gradient in California's Sierra Nevada, 117, https://doi.org/10.1029/2012JG002027, 2012.

Greenland, D.: The Climate of Niwot Ridge, Front Range, Colorado, U.S.A., 21, 380–391, https://doi.org/10.1080/00040851.1989.12002751, 1989.

Haario, H., Saksman, E., and Tamminen, J.: An adaptive Metropolis algorithm, Bernoulli, 7, 223–242, 2001.

Hu, J., Moore, D. J. P., Burns, S. P., and Monson, R. K.: Longer growing seasons lead to less carbon sequestration by a subalpine forest, 16, 771–783, https://doi.org/10.1111/j.1365-2486.2009.01967.x, 2010.

Huxman, T. E., Turnipseed, A. A., Sparks, J. P., Harley, P. C., and Monson, R. K.: Temperature as a control over ecosystem CO2 fluxes in a high-elevation, subalpine forest, Oecologia, 134, 537–546, https://doi.org/10.1007/s00442-002-1131-1, 2003.

Ishida, A., Nakano, T., Sekikawa, S., Maruta, E., and Masuzawa, T.: Diurnal changes in needle gas exchange in alpine Pinus pumila during snow-melting and summer seasons, 16, 107–116, https://doi.org/10.1046/j.1440-1703.2001.00376.x, 2001.

Jung, M., Reichstein, M., Schwalm, C. R., Huntingford, C., Sitch, S., Ahlström, A., Arneth, A., Camps-Valls, G., Ciais, P., Friedlingstein, P., Gans, F., Ichii, K., Jain, A. K., Kato, E., Papale, D., Poulter, B., Raduly, B., Rödenbeck, C., Tramontana, G., Viovy, N., Wang, Y.-P., Weber, U., Zaehle, S., and Zeng, N.: Compensatory water effects link yearly global land CO 2 sink changes to temperature, 541, 516–520, https://doi.org/10.1038/nature20780, 2017.

Keenan, T. F., Davidson, E., Moffat, A. M., Munger, W., and Richardson, A. D.: Using model-data fusion to interpret past trends, and quantify uncertainties in future projections, of terrestrial ecosystem carbon cycling, 18, 2555–2569, https://doi.org/10.1111/j.1365-2486.2012.02684.x, 2012.

Keenan, T. F., Gray, J., Friedl, M. A., Toomey, M., Bohrer, G., Hollinger, D. Y., Munger, J. W., O'Keefe, J., Schmid, H. P., Wing, I. S., Yang, B., and Richardson, A. D.: Net carbon uptake has increased through warming-induced changes in temperate forest phenology, 4, 598–604, https://doi.org/10.1038/nclimate2253, 2014.

Knowles, J. F., Burns, S. P., Blanken, P. D., and Monson, R. K.: Fluxes of energy, water, and carbon dioxide from mountain ecosystems at Niwot Ridge, Colorado, 8, 663–676, https://doi.org/10.1080/17550874.2014.904950, 2015.

Knowles, J. F., Molotch, N. P., Trujillo, E., and Litvak, M. E.: Snowmelt-Driven Trade-Offs Between Early and Late Season Productivity Negatively Impact Forest Carbon Uptake During Drought, 45, 3087–3096, https://doi.org/10.1002/2017GL076504, 2018.

Korzukhin, M. D., Ter-Mikaelian, M. T., and Wagner, R. G.: Process versus empirical models: which approach for forest ecosystem management?, https://doi.org/10.1139/x26-096, 2011.

Lasslop, G., Reichstein, M., Papale, D., Richardson, A., Arneth, A., Barr, A., Stoy, P., and Wohlfahrt, G.: Separation of net ecosystem exchange into assimilation and respiration using a light response curve approach: critical issues and global evaluation, 16, 2009.

Lin, J. C., Mallia, D. V., Wu, D., and Stephens, B. B.: How can mountaintop CO_2 observations be used to constrain regional carbon fluxes?, 17, 5561–5581, https://doi.org/10.5194/acp-17-5561-2017, 2017.

López-Blanco, E., Exbrayat, J.-F., Lund, M., Christensen, T. R., Tamstorf, M. P., Slevin, D., Hugelius, G., Bloom, A. A., and Williams, M.: Evaluation of terrestrial pan-Arctic carbon cycling using a data-assimilation system, 10, 233–255, https://doi.org/10.5194/esd-10-233-2019, 2019.

Magney, T. S., Bowling, D. R., Logan, B. A., Grossmann, K., Stutz, J., Blanken, P. D., Burns, S. P., Cheng, R., Garcia, M. A., Köhler, P., Lopez, S., Parazoo, N. C., Raczka, B., Schimel, D., and Frankenberg, C.: Mechanistic evidence for tracking the seasonality of photosynthesis with solar-induced fluorescence, PNAS, 116, 11640–11645, https://doi.org/10.1073/pnas.1900278116, 2019.

Medlyn, B. E., Dreyer, E., Ellsworth, D., Forstreuter, M., Harley, P. C., Kirschbaum, M. U. F., Roux, X. L., Montpied, P., Strassemeyer, J., Walcroft, A., Wang, K., and Loustau, D.: Temperature response of parameters of a biochemically based model of photosynthesis. II. A review of experimental data, 25, 1167–1179, https://doi.org/10.1046/j.1365-3040.2002.00891.x, 2002.

Monson, R. K., Turnipseed, A. A., Sparks, J. P., Harley, P. C., Scott-Denton, L. E., Sparks, K., and Huxman, T. E.: Carbon sequestration in a high-elevation, subalpine forest, 8, 459–478, https://doi.org/10.1046/j.1365-2486.2002.00480.x, 2002.

Moore, D. J. P., Hu, J., Sacks, W. J., Schimel, D. S., and Monson, R. K.: Estimating transpiration and the sensitivity of carbon uptake to water availability in a subalpine forest using a simple ecosystem process model informed by measured net CO2 and H2O fluxes, Agricultural and Forest Meteorology, 148, 1467–1477, https://doi.org/10.1016/j.agrformet.2008.04.013, 2008.

Myneni, R. B., Keeling, C. D., Tucker, C. J., Asrar, G., and Nemani, R. R.: Increased plant growth in the northern high latitudes from 1981 to 1991, 386, 698–702, https://doi.org/10.1038/386698a0, 1997.

Parazoo, N. C., Arneth, A., Pugh, T. A. M., Smith, B., Steiner, N., Luus, K., Commane, R., Benmergui, J., Stofferahn, E., Liu, J., Rödenbeck, C., Kawa, R., Euskirchen, E., Zona, D., Arndt, K., Oechel, W., and Miller, C.: Spring photosynthetic onset and net CO2 uptake in Alaska triggered by landscape thawing, Glob Chang Biol, 24, 3416–3435, https://doi.org/10.1111/gcb.14283, 2018.

Parazoo, N. C., Magney, T., Norton, A., Raczka, B., Bacour, C., Maignan, F., Baker, I., Zhang, Y., Qiu, B., Shi, M., MacBean, N., Bowling, D. R., Burns, S. P., Blanken, P. D., Stutz, J., Grossman, K., and Frankenberg, C.: Wide Discrepancies in the Magnitude and Direction of Modelled SIF in Response to Light Conditions, 2020, 1–42, https://doi.org/10.5194/bg-2019-508, 2020.

Pierrat, Z., Nehemy, M. F., Roy, A., Magney, T., Parazoo, N. C., Laroque, C., Pappas, C., Sonnentag, O., Grossmann, K., Bowling, D. R., Seibt, U., Ramirez, A., Johnson, B., Helgason, W., Barr, A., and Stutz, J.: Tower-Based Remote Sensing Reveals Mechanisms Behind a Two-phased Spring Transition in a Mixed-Species Boreal Forest, 126, e2020JG006191, https://doi.org/10.1029/2020JG006191, 2021.

Quetin, G. R., Bloom, A. A., Bowman, K. W., and Konings, A. G.: Carbon Flux Variability From a Relatively Simple Ecosystem Model With Assimilated Data Is Consistent With Terrestrial Biosphere Model Estimates, 12, e2019MS001889, https://doi.org/10.1029/2019MS001889, 2020.

https://doi.org/10.5194/bg-2021-152
Preprint. Discussion started: 17 June 2021

716 Randerson, J. T., Field, C. B., Fung, I. Y., and Tans, P. P.: Increases in early season ecosystem uptake explain recent
717 changes in the seasonal cycle of atmospheric CO2 at high northern latitudes, 26, 2765–2768,
718 https://doi.org/10.1029/1999GL900500, 1999.
719
720 Raupach, M. R., Rayner, P. J., Barrett, D. J., DeFries, R. S., Heimann, M., Ojima, D. S., Quegan, S., and
721 Schmullius, C. C.: Model–data synthesis in terrestrial carbon observation: methods, data requirements and data
722 uncertainty specifications, 11, 378–397, https://doi.org/10.1111/j.1365-2486.2005.00917.x, 2005.
723
724 Reichstein, M., Falge, E., Baldocchi, D., Papale, D., Aubinet, M., Berbigier, P., Bernhofer, C., Buchmann, N.,
725 Gilmanov, T., Granier, A., Grünwald, T., Havránková, K., Ilvesniemi, H., Janous, D., Knohl, A., Laurila, T., Lohila,
726 A., Loustau, D., Matteucci, G., Meyers, T., Miglietta, F., Ourcival, J.-M., Pumpanen, J., Rambal, S., Rotenberg, E.,
727 Sanz, M., Tenhunen, J., Seufert, G., Vaccari, F., Vesala, T., Yakir, D., and Valentini, R.: On the separation of net
728 ecosystem exchange into assimilation and ecosystem respiration: review and improved algorithm, 11, 1424–1439,
729 https://doi.org/10.1111/j.1365-2486.2005.001002.x, 2005.
730
731 Richardson, A. D., Williams, M., Hollinger, D. Y., Moore, D. J. P., Dail, D. B., Davidson, E. A., Scott, N. A.,
732 Evans, R. S., Hughes, H., Lee, J. T., Rodrigues, C., and Savage, K.: Estimating parameters of a forest ecosystem C
733 model with measurements of stocks and fluxes as joint constraints, Oecologia, 164, 25–40,
734 https://doi.org/10.1007/s00442-010-1628-y, 2010.
735
736 Rowland, L., Hill, T. C., Stahl, C., Siebicke, L., Burban, B., Zaragoza-Castells, J., Ponton, S., Bonal, D., Meir, P.,
737 and Williams, M.: Evidence for strong seasonality in the carbon storage and carbon use efficiency of an Amazonian
738 forest, 20, 979–991, https://doi.org/10.1111/gcb.12375, 2014.
739
740 Schimel, D., Schneider, F. D., and JPL Carbon and Ecosystem Participants: Flux towers in the sky: global ecology
741 from space, New Phytologist, 224, 570–584, https://doi.org/10.1111/nph.15934, 2019.
742
743 Scott-Denton, L. E., Moore, D. J. P., Rosenbloom, N. A., Kittel, T. G. F., Burns, S. P., Schimel, D. S., and Monson,
744 R. K.: Forecasting net ecosystem CO2 exchange in a subalpine forest using model data assimilation combined with
745 simulated climate and weather generation, 118, 549–565, https://doi.org/10.1002/jgrg.20039, 2013.
746
747 Sippel, S., Forkel, M., Rammig, A., Thonicke, K., Flach, M., Heimann, M., Otto, F. E. L., Reichstein, M., and
748 Mahecha, M. D.: Contrasting and interacting changes in simulated spring and summer carbon cycle extremes in
749 European ecosystems, Environ. Res. Lett., 12, 075006, https://doi.org/10.1088/1748-9326/aa7398, 2017.
750
751 Smallman, T. L., Exbrayat, J.-F., Mencuccini, M., Bloom, A. A., and Williams, M.: Assimilation of repeated woody
752 biomass observations constrains decadal ecosystem carbon cycle uncertainty in aggrading forests, 122, 528–545,
753 https://doi.org/10.1002/2016JG003520, 2017.
754
755 Smith, W. K., Fox, A. M., MacBean, N., Moore, D. J. P., and Parazoo, N. C.: Constraining estimates of terrestrial
756 carbon uptake: new opportunities using long-term satellite observations and data assimilation, 225, 105–112,
757 https://doi.org/10.1111/nph.16055, 2020.
758
759 Stavros, E. N., Schimel, D., Pavlick, R., Serbin, S., Swann, A., Duncanson, L., Fisher, J. B., Fassnacht, F., Ustin, S.,
760 Dubayah, R., Schweiger, A., and Wennberg, P.: ISS observations offer insights into plant function, 1, 1–5,
761 https://doi.org/10.1038/s41559-017-0194, 2017.
762
763 Sun, Y., Frankenberg, C., Wood, J. D., Schimel, D. S., Jung, M., Guanter, L., Drewry, D. T., Verma, M., Porcar-
764 Castell, A., Griffis, T. J., Gu, L., Magney, T. S., Köhler, P., Evans, B., and Yuen, K.: OCO-2 advances
765 photosynthesis observation from space via solar-induced chlorophyll fluorescence, 358,
766 https://doi.org/10.1126/science.aam5747, 2017.
767
768 Thurner, M., Beer, C., Santoro, M., Carvalhais, N., Wutzler, T., Schepaschenko, D., Shvidenko, A., Kompter, E.,
769 Ahrens, B., Levick, S. R., and Schmullius, C.: Carbon stock and density of northern boreal and temperate forests,
770 23, 297–310, https://doi.org/10.1111/geb.12125, 2014.
771

https://doi.org/10.5194/bg-2021-152
Preprint. Discussion started: 17 June 2021

772 Turnipseed, A. A., Blanken, P. D., Anderson, D. E., and Monson, R. K.: Energy budget above a high-elevation
773 subalpine forest in complex topography, Agricultural and Forest Meteorology, 110, 177–201,
774 https://doi.org/10.1016/S0168-1923(01)00290-8, 2002.
775
776 Turnipseed, A. A., Anderson, D. E., Burns, S., Blanken, P. D., and Monson, R. K.: Airflows and turbulent flux
777 measurements in mountainous terrain: Part 2: Mesoscale effects, Agricultural and Forest Meteorology, 125, 187–
778 205, https://doi.org/10.1016/j.agrformet.2004.04.007, 2004.
779
780 Wang, Y.-P., Trudinger, C. M., and Enting, I. G.: A review of applications of model–data fusion to studies of
781 terrestrial carbon fluxes at different scales, Agricultural and Forest Meteorology, 149, 1829–1842,
782 https://doi.org/10.1016/j.agrformet.2009.07.009, 2009.
783
784 Wang, J., Zeng, N., and Wang, M.: Interannual variability of the atmospheric CO_2 growth rate: roles of precipitation
785 and temperature, 13, 2339–2352, https://doi.org/10.5194/bg-13-2339-2016, 2016.
786
787 Williams, M., Rastetter, E. B., Fernandes, D. N., Goulden, M. L., Wofsy, S. C., Shaver, G. R., Melillo, J. M.,
788 Munger, J. W., Fan, S.-M., and Nadelhoffer, K. J.: Modelling the soil-plant-atmosphere continuum in a Quercus–
789 Acer stand at Harvard Forest: the regulation of stomatal conductance by light, nitrogen and soil/plant hydraulic
790 properties, 19, 911–927, https://doi.org/10.1111/j.1365-3040.1996.tb00456.x, 1996.
791
792 Williams, M., Rastetter, E. B., Fernandes, D. N., Goulden, M. L., Shaver, G. R., and Johnson, L. C.: Predicting
793 Gross Primary Productivity in Terrestrial Ecosystems, 7, 882–894, https://doi.org/10.1890/1051-
794 0761(1997)007[0882:PGPPIT]2.0.CO;2, 1997.
795
796 Williams, M., Law, B. E., Anthoni, P. M., and Unsworth, M. H.: Use of a simulation model and ecosystem flux data
797 to examine carbon–water interactions in ponderosa pine, Tree Physiology, 21, 287–298,
798 https://doi.org/10.1093/treephys/21.5.287, 2001.
799
800 Williams, M., Schwarz, P. A., Law, B. E., Irvine, J., and Kurpius, M. R.: An improved analysis of forest carbon
801 dynamics using data assimilation, 11, 89–105, https://doi.org/10.1111/j.1365-2486.2004.00891.x, 2005.
802
803 Williams, M. W., Seastedt, T. R., Bowman, W. D., McKnight, D. M., and Suding, K. N.: An overview of research
804 from a high elevation landscape: the Niwot Ridge, Colorado Long Term Ecological Research programme, 8, 597–
805 605, https://doi.org/10.1080/17550874.2015.1123320, 2015.
806
807 Winchell, T. S., Barnard, D. M., Monson, R. K., Burns, S. P., and Molotch, N. P.: Earlier snowmelt reduces
808 atmospheric carbon uptake in midlatitude subalpine forests, 43, 8160–8168, https://doi.org/10.1002/2016GL069769,
809 2016.
810
811 Wutzler, T., Lucas-Moffat, A., Migliavacca, M., Knauer, J., Sickel, K., Šigut, L., Menzer, O., and Reichstein, M.:
812 Basic and extensible post-processing of eddy covariance flux data with REddyProc, 15, 5015–5030,
813 https://doi.org/10.5194/bg-15-5015-2018, 2018.
814
815 Wolf, S., Keenan, T. F., Fisher, J. B., Baldocchi, D. D., Desai, A. R., Richardson, A. D., Scott, R. L., Law, B. E.,
816 Litvak, M. E., Brunsell, N. A., Peters, W., and van der Laan-Luijkx, I. T.: Warm spring reduced carbon cycle impact
817 of the 2012 US summer drought, Proc Natl Acad Sci USA, 113, 5880, https://doi.org/10.1073/pnas.1519620113,
818 2016.
819
820 Xu, C., Liu, H., Williams, A. P., Yin, Y., and Wu, X.: Trends toward an earlier peak of the growing season in
821 Northern Hemisphere mid-latitudes, 22, 2852–2860, https://doi.org/10.1111/gcb.13224, 2016.
822
823 Yin, Y., Bloom, A. A., Worden, J., Saatchi, S., Yang, Y., Williams, M., Liu, J., Jiang, Z., Worden, H., Bowman, K.,
824 Frankenberg, C., and Schimel, D.: Fire decline in dry tropical ecosystems enhances decadal land carbon sink, Nat
825 Commun, 11, 1900, https://doi.org/10.1038/s41467-020-15852-2, 2020.
826